Applied Catalysis A: General xxx (2015) xxx–xxx

Contents lists available at ScienceDirect

Applied Catalysis A: General

journal homepage: www.elsevier.com/locate/apcata

Photocatalytic valorization of ethanol and glycerol over TiO_2 polymorphs for sustainable hydrogen production

Alessandro Beltram[a], Ismael Romero-Ocaña[a], Juan Josè Delgado Jaen[b], Tiziano Montini[a,*], Paolo Fornasiero[a]

[a] Department of Chemical and Pharmaceutical Sciences, ICCOM-CNR, Consortium INSTM, University of Trieste, via L. Giorgieri 1, 34127 Trieste, Italy
[b] Departamento de Ciencia de los Materiales e Ingeniería Metalúrgica y Química Inorgánica, Facultad de Ciencias, Universidad de Cádiz, Campus Río San Pedro, 11510, Puerto Real, Cádiz, Spain

ARTICLE INFO

Article history:
Received 24 July 2015
Received in revised form
14 September 2015
Accepted 16 September 2015
Available online xxx

Keywords:
Hydrogen
Photocatalysis
Titania
Ethanol
Glycerol

ABSTRACT

Photocatalytic reforming of renewable raw materials in aqueous solutions represents a valid possibility for the valorization of wastes from agricultural and industrial processes. In this study, we prepared TiO_2 materials with different phase compositions by changing the urea/Ti molar ratio employed during the hydrothermal preparation method. After deposition of Pt nanoparticles, the photocatalytic H_2 production was investigated using ethanol and glycerol as sustainable sacrificial agent. While anatase/rutile nanocomposites showed poor catalytic activity, the anatase/brookite nanocomposites showed more promising performances. Specifically, the anatase-rich materials showed the best performances on mass bases. When normalized with respect to the surface area of the photocatalysts, the activity continuously increased with the brookite content, indicating that exposed facets of brookite possess an intrinsic higher activity than that of the other polymorphs.

1. Introduction

Hydrogen is an essential molecule for chemical industry, being involved in important processes (ammonia synthesis, oil refinery etc.,) as well as in the production of high added-value compounds [1]. Nowadays, H_2 is produced principally by steam reforming of natural gas, coal or crude oil. Only marginal amounts are obtained by reforming of biofuels or by electrolysis [2,3]. All the processes involved in H_2 production require the supply of large amounts of external energy, since all the reactions producing H_2 (steam reforming, water splitting) are endothermic ($\Delta H > 0$) and endoergonic processes ($\Delta G > 0$).

The sustainability of H_2 production will be improved satisfying two conditions. First, the molecule from which hydrogen is extracted must be renewable, cheap and available worldwide in large quantities. The best candidates are water and second or next generation biomasses, the use of which also limit anthropogenic CO_2 emission into the atmosphere [4–8]. Second, clean primary energy sources must be employed, i.e. biofuels or solar, wind, tidal or geothermal energy [2,3,9,10].

Many technologies using solar light as primary energy sources have been considered, such as electrolysis of water coupled with photovoltaic electrical energy [9,11], water splitting by photoelectrochemical [12–15], thermochemical [16,17] or photochemical processes [12,18] and photoreforming of renewable oxygenated compounds [19,20]. This last possibility is thermodynamically more efficient with respect to water splitting and opens the possibility to produce H_2 in combination with the clean-up of waste aqueous streams from food, wine or paper industry [21].

In this context, TiO_2 represents the most investigated semiconductor material because of its chemical stability, its low cost and large availability [22,23]. The quite large band gap of TiO_2 polymorphs (3.0–3.3 eV) allowing this material to be active only using UV photons and the fast recombination of photogenerated electron/hole pairs represent the main drawbacks limiting the performances. Many strategies have been adopted to improve performances of TiO_2 materials increasing the lifetime of electron/hole pairs and/or extending the responsive range to visible light, such as doping [24–42], formation of composites with another semiconductor [43–47] or metal nanoparticles [48–53]. This last option opens the possibility to harvest visible light through plasmonic resonance of metal nanoparticles [54–60].

The different polymorphs of TiO_2 show quite different photocatalytic activity, especially in H_2 production processes. Taking

---

* Corresponding author.
E-mail address: tmontini@units.it (T. Montini).

http://dx.doi.org/10.1016/j.apcata.2015.09.022

the most studied phase — anatase and rutile — as examples, the differences in crystal structure result in different densities and electronic band structure. Anatase has a larger band gap of rutile (3.20 vs 3.02 eV), resulting in slightly higher conduction band edge energy and electron Fermi level [22,23]. Due the lower density, the Ti–Ti distance in anatase is larger than in rutile, resulting in more localized 3d states [61,62]. Generally, anatase has larger surface area than rutile, favoring adsorption of molecules and increasing the activity because of the higher number of active sites. Finally, the smaller crystallite size of anatase improves the efficiency of electron/hole generation while the higher crystallinity of rutile favor charge mobility [22]. The photocatalytic properties of brookite, another polymorph of TiO_2, attracted great attention in the last years. Particular advantage has been reported by the use of brookite-containing materials in H_2 production from aqueous solution containing methanol [63–65] or ethanol [66]. These results have been related with the larger band gap of brookite (3.3–3.4 eV), lying the edge of its conduction band to higher potential with respect to anatase [65].

In this study, we employed a thermal hydrolysis process to prepare crystalline TiO_2 materials with different phase composition, tuned changing systematically the synthesis conditions. Adopting the same reaction conditions (160 °C, 24 h) and the same Ti precursor (titanium (IV) bis(ammonium lactate) dihydroxide — $Ti(NH_4C_3H_4O_3)_2(OH)_2$) and changing the urea concentration employed for hydrolysis (0–7.0 M), the phase composition can be tuned depending on the urea/Ti molar ratio, ranging from rutile to anatase and finally pure brookite, through the formation of the biphasic composites (rutile/anatase and anatase/brookite). These materials have been tested for photocatalytic H_2 production under simulated sunlight employing renewable raw materials as sacrificial agents: ethanol and glycerol.

2. Experimental

2.1. Catalyst preparation

TiO_2 nanomaterials with different phase composition were synthesized by hydrothermal treatment from commercial titanium (IV) bis(ammonium lactate) dihydroxide $Ti(NH_4C_3H_4O_3)_2(OH)_2$ aqueous solution (50 wt%, Sigma–Aldrich) in the presence of urea, adapting the procedure reported by Zhao et al. [67]. A 40 mL Teflon-lined autoclave was charged with 1.5 mL of the Ti based precursor and 13.5 mL of urea solution. The concentration of urea solution was systematically increased from 0 to 7.0 M, in order to obtain urea/Ti molar ratios in the range 0 – 44.5. After careful mixing, the autoclave was heated at 160 °C for 24 h in a convection oven. The product is obtained as a precipitate with a color changing from slightly yellow to white as the urea/Ti molar ratio increases. The precipitate was collected by centrifugation, washed several times with bi-distilled water and finally dried at 80 °C overnight. The materials were subjected to calcination at 400 °C for 3 h in order to remove any organic contaminants deriving from partial decomposition of the lactate precursor, obtaining white solids. Hereafter, the obtained TiO_2 materials are labeled as T-X, where X is the urea/Ti molar ratio.

2.2. Materials characterization

X-ray diffraction (XRD) patterns were collected on a Philips X'Pert diffractometer using a monochromatized Cu Kα ($\lambda = 0.154$ nm) X-ray source in the range $10° < 2\theta < 100°$ and data were analyzed using the PowderCell 2.0 software. Mean crystallite sizes were calculated applying the Scherrer equation to the principal reflection of each phase.

The morphology of the composite materials was investigated by high resolution TEM (HR-TEM) measurements, performed on a TEM JEOL 2010-FEG microscope with an acceleration voltage of 200 kV and with 0.19 nm spatial resolution at Scherzer defocus conditions. In order to obtain accurate particle size distribution of the photodeposited Pt nanoparticles, High-Angle Annular Dark-Field (HAADF)—Scanning Transmission Electron Microscopy (STEM) technique was carried out using an electron probe of 0.5 nm and a diffraction camera length of 120 cm. HAADF-STEM allows to obtain Z-contrat images and easily identify heavy metals on light support. At least 150 particles were counted to obtain the particle size distribution. The samples collected after the catalytic tests were washed with a water/ethanol solution, dried and dispersed onto lacey carbon grid.

N_2 physisorption measurements at the liquid nitrogen temperature was performed using a Micrometrics ASAP 2020 automatic analyzer. The samples were degassed in vacuum at 120 °C for 12 h prior to analysis.

2.3. Photocatalytic tests

The activity of the prepared materials was evaluated in terms of hydrogen production by photoreforming of two alcohols of relevant environmental interest present in aqueous solution: ethanol at 50% v/v and glycerol 1 M.

In a Teflon-lined photoreactor described elsewhere [68], 50 mg of the calcined materials were suspended into 80 mL of alcohol solution containing 100 μL of an aqueous solution of $Pt(NO_3)_2$ (1 mg Pt mL^{-1}). The amount of the catalyst has been optimized following the indication recently reported by Kisch and Bahnemann [69]. Before switching on the lamp, the reactor was thermostated at 25 °C and purged from the air with Ar flow of 15 mL min^{-1} for at least 40 min. The photoreactor was illuminated with a Lot-Oriel Solar Simulator equipped with a 150 W Xe lamp and an Atmospheric Edge Filter with a cut-off at 300 nm. This results in a surface power density of ~25 mW cm^{-2} in the UV range (300–400 nm) and ~180 mW cm^{-2} in the visible range (400–100 nm), approaching the conditions used in a solar concentrator. During the initial part of the photocatalytic experiments, Pt nanoparticles were loaded as co-catalysts on the surface of the TiO_2 materials, reaching a final loading of 0.2 wt%.

The on-line detection of volatile products was carried out using an Agilent 7890A Gas Chromatograph equipped with two analytical lines. A 10 way-two loops injection valve was employed for injection during on-line analysis of the gaseous products. A Carboxen 1010 PLOT (Supelco, 30 m × 0.53 mm ID, 30 μm film) column followed by a Thermal Conductivity Detector (TCD) was used for gaseous products quantification using Ar as carrier and a DB-225ms column (J&W, 60 m × 0.32 mm ID, 20 μm film) using He as carrier followed by a mass spectrometer (MS) HP 5975C was employed for the detection of the volatile organic compounds.

After photocatalytic runs, the catalysts were collected by filtration on a 0.45 μm PVDF Millipore membrane in order to analyze the Pt nanoparticles distribution on the materials while the solutions recovered were analyzed by GC/MS to detect the by-products accumulated in the liquid phase. For a semi-quantitative analysis, 1-butanol and 1-hexanol were used as internal standards in samples from photoreforming of ethanol and glycerol, respectively.

Possible leaching of Pt during photocatalytic runs was checked by Graphitic Furnace—Atomic Absorption Spectroscopy (GF-AAS) using a Thermo M series AA spectrometer equipped with a GF95Z Zeeman Furnace and a FS95 Furnace Autosampler (Thermo Electron Corporation, Cambridge, UK). Pt detection limit at the analytical wavelength of 266.0 nm was 10 μg/L. A five-point standard curve (in the range of 10–1000 μg/L) was used for the analytical measurements. The correlation coefficient of the standard curve was at least

Please cite this article in press as: A. Beltram, et al., Appl. Catal. A: Gen. (2015), http://dx.doi.org/10.1016/j.apcata.2015.09.022

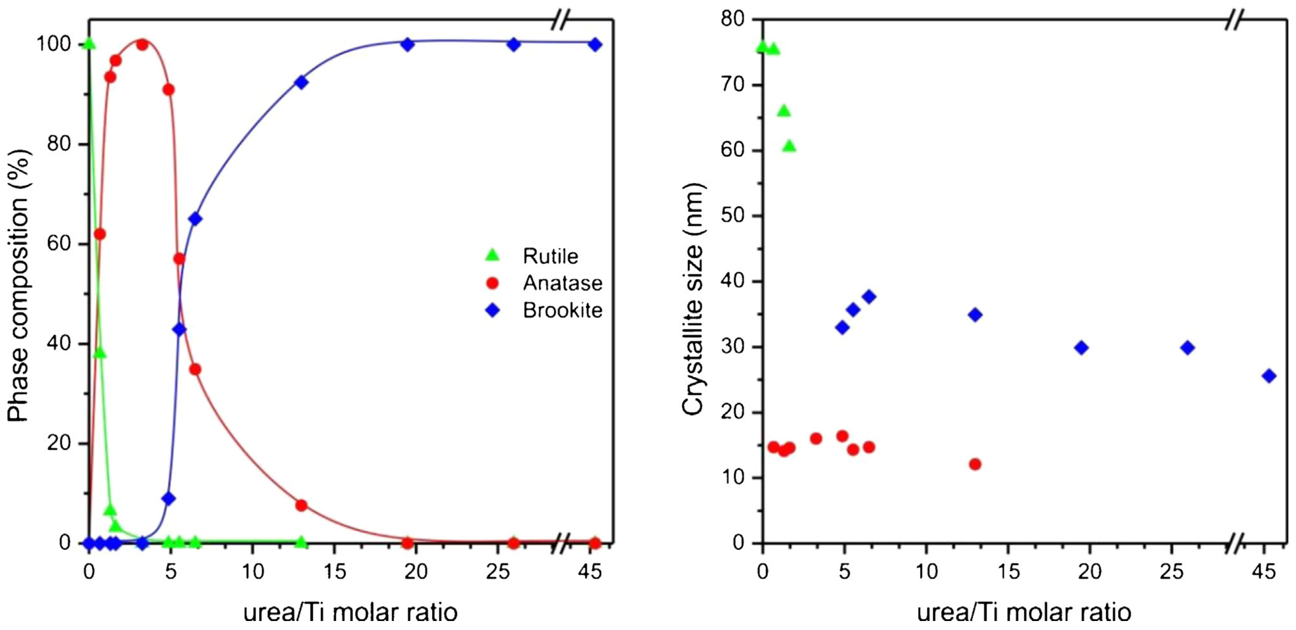

Fig. 1. Evolution of phase composition (left part) and mean crystallite sizes (right part) as a function of the initial urea concentration during the hydrothermal treatment.

0.9995. The samples were analyzed measuring against standard solutions for instrumental calibration. The precision of the measurements as relative standard deviation (RSD%) for the analysis was always less than 5%.

3. Results and discussion

3.1. Phase composition: powder XRD analysis

Significant variations of the phase composition of the TiO_2 materials were observed as a function of the concentration of urea employed in the hydrothermal synthesis.

All the samples present well developed XRD patterns (Fig. S1), indicating the absence of amorphous material. Notably, un-calcined samples show sharp and very similar XRD profiles, indicating that the crystallization process effectively occurs during the hydrothermal treatment and suggesting that calcination is required only to remove minor residual organic moieties. Rietveld analysis was performed to estimate phase composition and cell parameters. Fits with very good quality were obtained for all the samples (Fig. S1). Fig. 1 and Table 1 summarize the evolution of the phase composition determined by Rietveld analysis and of the mean crystallite sizes for the different phases detected as a function of the initial urea/Ti molar ratio employed. The corresponding cell parameters of the different phases obtained from Rietveld analysis are summarized in Table S1. Notably, no significant difference between the tabulated and the experimental cell parameters have been observed, in agreement with the good crystallinity and the absence of significant amount of defects within the crystal structure of the particles.

As reported in Table 1 and Fig. 1, the three TiO_2 polymorphs can be prepared in a pure form selecting the adequate urea/Ti molar ratio: zero for rutile (hydrolysis of Ti precursor in pure water) and 3.25 for anatase while every urea/Ti molar ratio above 19.5 produces brookite. At intermediate values, mixtures of two polymorphs are obtained, changing from rutile/anatase composites to anatase/brookite composites. The formation of anatase/brookite composite has been already reported using similar preparation methodology (although with some differences in conditions adopted and results — see below) [67], the preparation of pure rutile and rutile/anatase composites is reported here for the first time.

The effect of preparation parameters of TiO_2 materials by solution-based methods on the final phase composition has been widely investigated in the literature, as recently reviewed by Kumar and Rao [70]. The thermolysis (hydrolysis induced by thermal treatment) of $Ti(NH_4C_3H_4O_3)_2(OH)_2$ in the presence of urea has been reported in the literature for the preparation of TiO_2 in the anatase/brookite composition range [67]: pure anatase has been produced at the lower urea concentration while pure brookite is obtained increasing urea amount. This results has been related with the in situ hydroxide ions dosing, favoring brookite formation at the higher hydroxide concentrations. This is in agreement with the effect of pH on the hydrothermal treatment applied to hydrolyzed $Ti(O\text{-}n\text{-}Bu)_4$ [71]: increasing pH of the solution, various Ti-based materials can be obtained in the sequence rutile–anatase–brookite–$Na_2Ti_2O_5$–$Na_3Ti_2O_7$. In our case, the phase composition obtained by the thermolysis of $Ti(NH_4C_3H_4O_3)_2(OH)_2$ slightly differ from what reported by Zhao et al. [67], although comparable urea concentrations have been employed. Our group have recently reported how the composition of the products of a hydrothermal treatment depends on parameters such as autoclave free volume, heating and cooling method etc [66]. The difference in phase composition observed in this study

Table 1
Phase composition and mean crystallite sizes calculated from the XRD patterns analysis.

Sample	Phase composition (wt%)			Average crystallite size (nm)		
	Rutile	Anatase	Brookite	Rutile	Anatase	Brookite
T-0	100	0	0	75.7	0	0
T-0.65	38	62	0	75.3	14.7	0
T-1.30	6.5	93.5	0	65.9	14.1	0
T-1.62	3.2	96.8	0	60.5	14.6	0
T-3.25	0	100	0	0	16.0	0
T-4.87	0	91	9	0	16.4	33.0
T-5.52	0	57.1	42.9	0	14.3	35.7
T-6.49	0	34.9	65.1	0	14.7	37.7
T-13.0	0	7.6	92.4	0	12.1	34.9
T-19.5	0	0	100	0	0	29.9
T-26.0	0	0	100	0	0	29.9
T-45.4	0	0	100	0	0	25.6

Please cite this article in press as: A. Beltram, et al., Appl. Catal. A: Gen. (2015), http://dx.doi.org/10.1016/j.apcata.2015.09.022

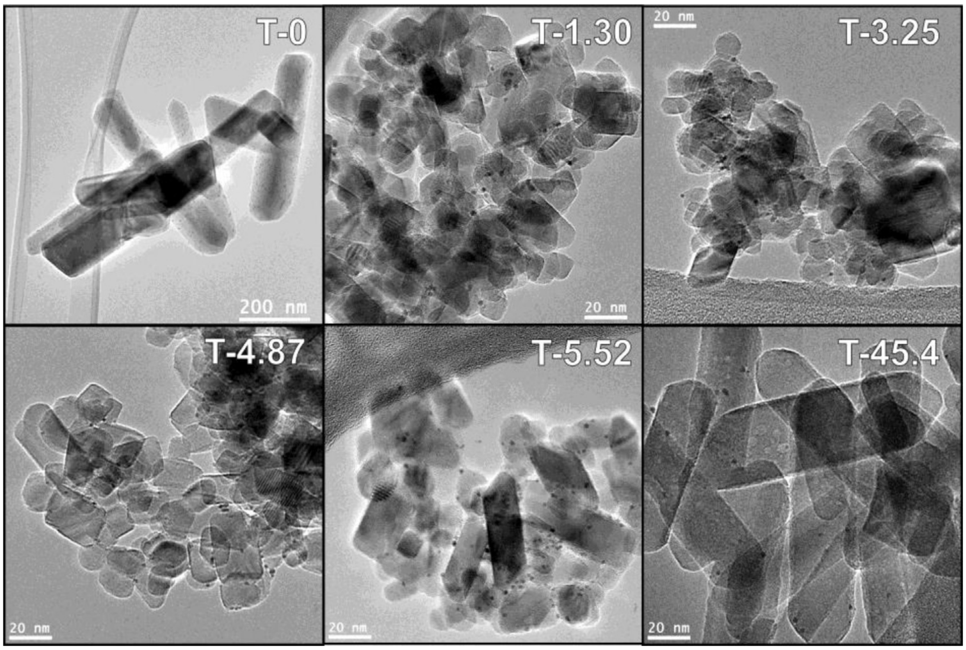

Fig. 2. Representative TEM micrographs of selected Pt(0.2 wt%)/TiO_2 nanocomposites, showing the evolution of the morphology of the TiO_2 materials with the initial urea/Ti molar ratio.

can be therefore related with slightly different conditions in all these synthetic parameters with respect to the conditions adopted by Zhao et al. [67]. In particular, the formation of rutile could be associated with a decrease of the pH of the solution associated to lactate decomposition, as assessed by the yellowish color of the un-calcined products obtained at the lower urea/Ti molar ratios. Release of CO_2 by lactate decomposition can lower the pH of the solution, favoring rutile formation. This is particularly evident in the thermolysis of $Ti(NH_4C_3H_4O_3)_2(OH)_2$ in the absence of urea (sample T-0), leading to pure rutile formation. In agreement with this, pure anatase formation is observed at higher urea concentration with respect to the previous report [67] (0.5 M instead of 0.1 M). On the other hand, formation of pure brookite is observed in a wide range of urea/Ti molar ratios (correspondents to urea concentration higher than 3.0 M) while Zhao et al. [67] did not report any other conditions intermediate between 1.5 and 7.0 M.

3.2. Morphological characterization: TEM analysis

The morphology of the TiO_2 materials was analyzed by TEM analysis of the samples. Representative images of selected samples are presented in Fig. 2. The morphology of the produced TiO_2 materials are also significantly influenced by the initial urea concentration used in the hydrothermal synthesis, reflecting the above discussed evolution of the phase composition. All the samples present well defined particles. The pure rutile phase (Fig. 2, T-0) shows the presence of very large crystallites, with a mixture of rods and polyhedral particles, with sizes from tens to hundreds nanometers. The pure anatase phase (Fig. 2, T-3.25) is composed of crystallites with irregular shape, the most of them with dimensions in the 10–20 nm range. The pure brookite phase obtained for urea/Ti molar ration higher than 19.5 is obtained as nanorods with lengths of 80–100 nm and widths of 20–40 nm (Fig. 2, T-45.4). The nanorods have a square section and terminate with 2 piramids. This is in agreement with previous preparation of brookite phase [67].

In the materials prepared at intermediate urea/Ti molar ratios, the presence of the two TiO_2 polymorphs can be distinguished also from the morphological analysis. The rutile/anatase composites (Fig. 2, T-1.30) are composed by crystallites with irregular shape with size in the 10–20 nm range together with an appreciable fraction of larger crystallites. Accordingly to the mean crystallite sizes calculated from the analysis of XRD patterns, the smallest particles should be recognized as anatase while the largest should be related with the rutile phase. The anatase/brookite composites (Fig. 2, T-4.87 and T-5.52) show the presence of mixtures of nanorods, related to the brookite phase, and small crystallites with size around 10–20 nm, assigned as anatase.

The Pt nanoparticles deposited on the surface of the prepared TiO_2 materials can be observed as bright spots in the HAADF-STEM images presented in Fig. 3. The particles are well dispersed on the surface of the TiO_2 and no appreciable aggregates are observed. Notably, in the case of brookite-pure sample (T-45.4), Pt nanoparticles are observed on the lateral surfaces of the nanorods. This is in agreement with previous reports accounting for accumulation of electrons on lateral surfaces [72], where they are initially consumed for reduction of Pt^{2+} ions and nucleation/growth of the nanoparticles. The size distribution of representative samples after photodeposition in water/ethanol solutions are presented in Fig. 3, observing that Pt nanoparticles in the range of 1–3 nm are obtained for all the samples. This result is in agreement with previous reports [66] and is related with the favored electron/hole separation realized at the boundary between crystallites. Notably, no significant differences were observed for Pt nanoparticles photodeposited during experiments in water/glycerol solutions, indicating that the size of Pt nanoparticles in mainly influenced by the composition of the photoactive TiO_2 support and not by the nature of the sacrificial agent employed.

3.3. Textural characterization: N_2 physisorption

The textural properties on the obtained materials were analyzed by N_2 physisorption at the liquid nitrogen temperature. The rutile sample prepared in the absence of urea shows a Type II isotherm (Fig. S2), typical of non porous/macroporous materials [73], leading to a low surface area (~7 m^2/g). All the other materials show Type IV isotherms (Fig. S2), typical of mesoporous materials [73], with shapes affected by the initial urea/Ti molar ratio adopted in the preparation (Fig. S2). The samples prepared at the lowest urea/Ti

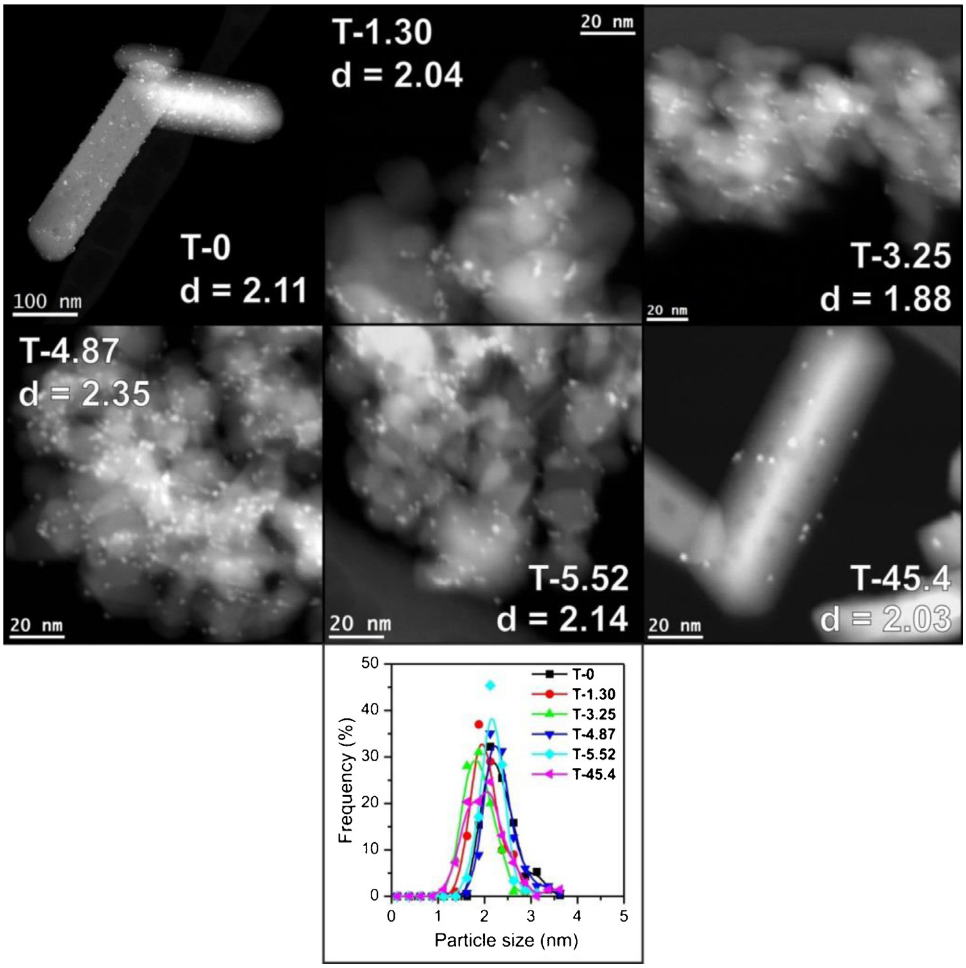

Fig. 3. Representative HAADF-STEM micrographs of selected Pt(0.2 wt%)/TiO_2 samples and size distribution of the Pt nanoparticles after photodeposition in ethanol/water solutions.

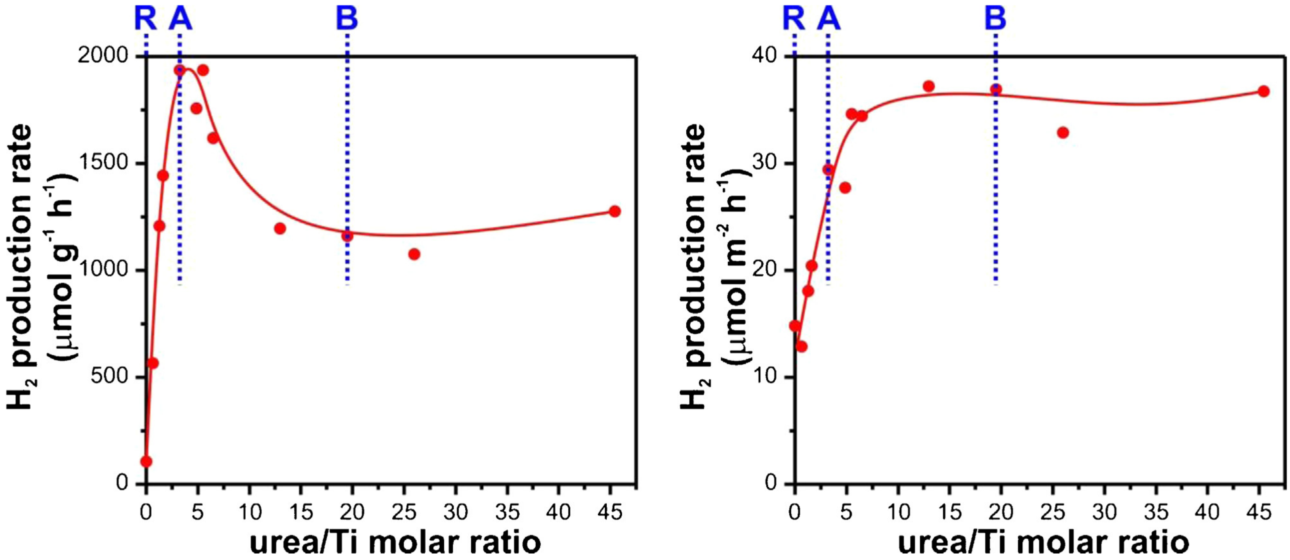

Fig. 4. Stable H_2 production rate by photocatalytic ethanol dehydrogenation using Pt(0.2 wt%)/TiO_2 prepared using different urea/Ti molar ratios, normalized with respect to the mass of catalysts (left part) and with respect the surface area (right part). Markers correspond to the urea/Ti molar ratios that allow the preparation of pure phase materials: rutile (R), anatase (A) and brookite (B).

molar ratios (T-0.65–T-5.52) show type H3, typical of aggregates of particles giving rise to slit-shaped pores. In agreement with this, TEM analysis evidenced the formation of aggregates of particles with irregular shape. As the urea/Ti molar ratio increases (T-6.49–T-45.4), the shape of the hysteresis loop changes to type H1, usually associated with the formation of agglomerates of particles of uniform sizes and shapes finally leading to narrow pore size distribution. This is in agreement with the analysis of morphology

Please cite this article in press as: A. Beltram, et al., Appl. Catal. A: Gen. (2015), http://dx.doi.org/10.1016/j.apcata.2015.09.022

Table 2
Results from N_2 physisorption analysis of the investigated samples.

Sample	Specific surface area ($m^2\,g^{-1}$)[a]	Cumulative pore volume ($mL\,g^{-1}$)	D_{max} (nm)[b]
T-0	7.2	0.024	>100
T-0.65	44	0.235	15.5
T-1.30	67	0.278	14.1
T-1.62	71	0.287	14.5
T-3.25	66	0.309	15.0
T-4.87	63	0.306	15.1
T-5.52	56	0.267	17.6
T-6.49	47	0.290	22.4
T-13.0	32	0.320	38.9
T-19.5	31	0.370	39.4
T-26.0	33	0.375	38.6
T-45.4	35	0.366	36.9

[a] Calculated from the BET analysis of the isotherms.

[b] Relative maximum of the pore size distributions obtained by the BJH analysis of the desorption branch of the isotherms.

performed by TEM. In fact, as the urea/Ti molar ratio increases, the formation of brookite nanorods were observed, allowing the packing of the particles with a certain order.

Specific surface area, cumulative pore volume and maximum of pore size distribution are summarized in Table 2 while the pore size distribution obtained from the BJH analysis of the desorption branch of the N_2 physisorption isotherms are reported in Fig. S3. As the urea/Ti molar ratio progressively increases, peculiar modification can be observed in the textural properties of the samples. The very low surface area presented by the T-0 sample is in agreement with the very large crystallite size of the pure rutile material. The surface area of the materials is higher for anatase-rich samples (T-1.30–T-4.87) and progressively decreases as the brookite content increases (T-5.52–T-45.4). At the same time, modifications are observed in the porous network, in terms of both pore volume and size distribution. The cumulative pore volume has a relative maximum for the pure anatase sample (T-3.25), decreasing and then increasing again with the brookite content reaching a maximum for the pure brookite samples (T-19.5–T-45.4). At the same time, the pore size distributions have a maximum around 15 nm until the brookite content becomes significant (T-5.52), progressively enlarging to 37–39 nm for the pure brookite samples.

The largest surface area and pore volume, together with the relatively small pore diameters presented by anatase-reach samples (T-1.62–T-4.87) are in perfect accordance with the small crystallize size of the anatase phase. Vice versa, the larger crystallite sizes of rutile and brookite significantly reduce the surface area of the corresponding materials. On the other hand, the largest pore volume and pore size of the pure brookite samples is justified by the formation of agglomerates of the large nanorods, which possess a limited specific surface area but stack together leaving large voids between the particles.

3.4. *Functional characterization: photocatalytic activity in H_2 production through ethanol and glycerol photoreforming*

H_2 production from photoreforming of renewable raw materials was used as test for the performances of the present TiO_2 materials. Ethanol/water 50/50 solution was used as a representative product obtained from fermentation of agricultural and/or municipal wastes, followed by a primary purification by distillation. Glycerol/water 1 M solution is representative of a purified solution produced as by-product in biodiesel production plants [74]. The photocatalytic experiments evidenced that the H_2 production is strongly dependent from synthetic condition adopted in the preparation of the TiO_2 materials, using both ethanol/water or glycerol/water solutions.

The temporal evolution of the H_2 production rates from ethanol /water solutions (Fig. S4, left part) show an initial increment during the initial 2–3 h of reaction. During this induction period, activation of the catalysts is observed, involving deposition of the Pt nanoparticles by photoreduction of Pt^{2+}ions. After the activation period, the H_2 production rate slightly decreases with time of irradiation. This deactivation depends on the phase composition of the TiO_2. The samples with the higher brookite content (prepared at the higher urea/Ti molar ratio) result the more stable. The decrease in H_2 production rate is a phenomenon already observed for Pt/TiO_2 photocatalysts and it is associated to the strong adsorption of by-products of partial oxidation of the alcohol on the surface of Pt nanoparticles [75]. The analysis of aqueous solutions recovered at the end of photocatalytic runs by GF-AAS did not show the presence of appreciable amounts of Pt, indicating that the co-catalyst is completely deposited on the surface of TiO_2 materials and that the amount leached during prolonged irradiation is negligible (the limit of detection of 10 μg/L corresponds to 0.8 % of total Pt added before photodeposition).

Fig. 4 reports the averaged H_2 production rates during the last 5 h of the photocatalytic experiments using ethanol as sacrifical agent. When normalized with respect to the mass of the photocatalyst (Fig. 4, left part), highest H_2 production rates are observed for the anatase-reach materials (T-3.25–T-5.52). The presence of rutile leads to a significant drop in activity. This in agreement with previous reports on photocatalytic H_2 production from aqueous methanol using anatase/rutile composites [76,77]. Anatase possesses higher conduction band edge energy and Fermi level than rutile and lower electron–hole recombination rate [78]. Studying photoactivity of P25, Hurum et al. proposed that, in the anatase/rutile composite materials, increased lifetime of electron/hole pairs is associated to the migration of the photoexcited electrons from the conduction band of anatase the that of rutile, lying this at a lower potential [79]. Although this is beneficial in the case of organic molecule degradation, a negative effect is expected for H_2 production, since the potential of electrons in the conduction band could become too low to reduce protons. In agreement with these observations, Murdoch et al. studied the H_2 photoproduction from ethanol/water solutions using Au/TiO_2 in the forms of anatase and rutile [80]. Normalizing the H_2 production rate normalized on the surface area of the materials, the activity using anatase is ~100 times higher than that observed using rutile.

In the series of anatase/brookite samples, the best activities are observed for composites up to brookite content a brookite content of ~40 wt% (T-3.25–T-5.52) and progressively decreases up to pure brookite. The best performances of brookite/anatase composites in photocatalytic H_2 production has been related with the more cathodic conduction band edge potential, allowing electron transfer to anatase phase and increasing lifetime of photogenerated electron–hole pairs [65]. A maximum in H_2 production from methanol/water solutions was recently reported for anatase/brookite composites around 36 wt% of brookite by Cihlar et al. [63] or around 11.5 wt% by Tay et al. [65]. We have recently reported that anatase/brookite composites prepared from Na-titanate precursor showed higher activity than pure anatase using aqueous ethanol solutions [66]. In all these cases, the promotional effect due to anatase/brookite TiO_2 materials is evident considering that comparable surface areas were measured for pure anatase and for the composite materials [63,65,66]. In the present case, we face a significant change in the surface area of the various sample, and its negative decrease with the increase of brookite content can be compensated by the positive compositional effect, keeping comparable activities in the range 0–40 wt% of brookite. In fact, normalizing the H_2 production rate with respect to the surface

Please cite this article in press as: A. Beltram, et al., Appl. Catal. A: Gen. (2015), http://dx.doi.org/10.1016/j.apcata.2015.09.022

area of the materials (Fig. 4, right part), brookite-rich materials show the best performances.

The direct comparison of photocatalytic activity is not simple when significant variation of crystallite sizes and surface area are observed among the samples. On the other hand, the synthesis of TiO_2 materials with different phase composition and comparable crystallite sizes is not a simple task, especially considering that phase stability strongly depends on the dimension of the crystallites [81]. This problem could be overcome normalizing the H_2 production rates on the surface area of the TiO_2 materials. Nadeem et al. highlighted that the activity of Au/TiO_2 anatase in photoproduction of H_2 from ethanol normalized on the surface area does not depend on crystallite size of anatase [82]. This result demonstrates that the improvement of activity with decrease of crystallite size is simply a geometrical effect in the case of anatase [82]. Although this was demonstrated only for materials containing pure anatase, it is expected that significant differences on the reaction rates normalized on the surface are can be related with intrinsic electronic properties of the materials investigated.

In this study, we observed a significant improvement of H_2 production rate for brookite with respect to rutile and anatase when normalized on the surface area of the materials. This result can be rationalized considering the well-defined morphology of brookite phase, resulting in a more efficient electron–hole separation. Consistently, it has been demonstrated that photogenerated electrons and holes accumulates on different exposed facets and that the charge separation is favored by materials with controlled morphologies [72,83,84].

When ethanol is used as sacrificial agent, H_2 is produced by photocatalytic dehydrogenation of the organic molecule, producing acetaldehyde and its acetal (1,1-diethoxyethane) as major by-products. No other by-products have been detected. It is recognized that acetaldehyde is produced by oxidation of ethoxide species, formed by dissociative adsorption of ethanol on the surface of TiO_2, consuming the holes produced by irradiation of the photoactive material [20,66,85]. The majority of these compounds is accumulated in the liquid phase (Table S2), as revealed by the analysis of the solutions recovered after photocatalytic experiments, while only vapors can be detected in trace amounts in the gas stream from the reactor. The amounts of acetaldehyde and 1,1-diethoxyethane follow the same trend observed for H_2 production, with the higher concentrations for the anatase-rich materials. No other gaseous by-products, such as CO_2, CO or CH_4, have been detected, in agreement with previous reports [53,66]. This is due to the low capability of acetaldehyde and its derivatives to be adsorbed on the surface of TiO_2.

During photocatalytic reforming of an aqueous solution containing glycerol as sacrificial agent, both H_2 and CO_2 evolution was observed by the on-line analysis of the gas stream coming from the photoreactor. The only exception to this general trend is the case of the T-0 sample, containing pure rutile, showing no production of CO_2. Also in the case of glycerol, an activation period is observed in the H_2 production rate (Fig. S5, left part): the maximum rate is reached after 1.5–3.5 h, depending on the composition of the TiO_2 material. Also in the case of glycerol, after the initial activation period required for Pt nanoparticles deposition, the H_2 production rates decreases with irradiation time. The extent of the deactivation in the case of glycerol photoreforming is higher than that observed during H_2 photoproduction from ethanol. Again, brookite-rich materials show the most stable activities. At the same time, the evolution of CO_2 shows an activation period longer than that of H_2 and, after the first 4–5 h of irradiation, the CO_2 production rates remain constant or slightly increase during the rest of the photocatalytic runs. CO_2 evolution is observed in the case of glycerol photoreforming thanks to a complex network of consecutive reactions, finally leading to the complete mineralization of the organic skeleton [53]. As a consequence, the CO_2 evolution is delayed with respect to the H_2 production since CO_2 derives from decarboxylation steps involving the by-products accumulated in the aqueous solution during glycerol photoreforming. Notably, CO and CH_4 have not been detected in the gas phase, indicating that degradation of the organic skeleton is very selective with respect to the decarboxylation reaction. On the other hand, production of CO and CH_4 is often observed when more powerful light sources are employed, i.e. Hg lamps for UV–vis irradiation [52,86]. Also in this case, GF-AAS analysis of the solutions recovered after photocatalytic runs did not show the presence of appreciable amounts of Pt, indicating that deactivation observed cannot be related with leaching of the co-catalyst added during photodeposition.

Fig. 5 presents the stable H_2 and CO_2 production rates averaged in the last 5 h of the photocatalytic runs as a function of the

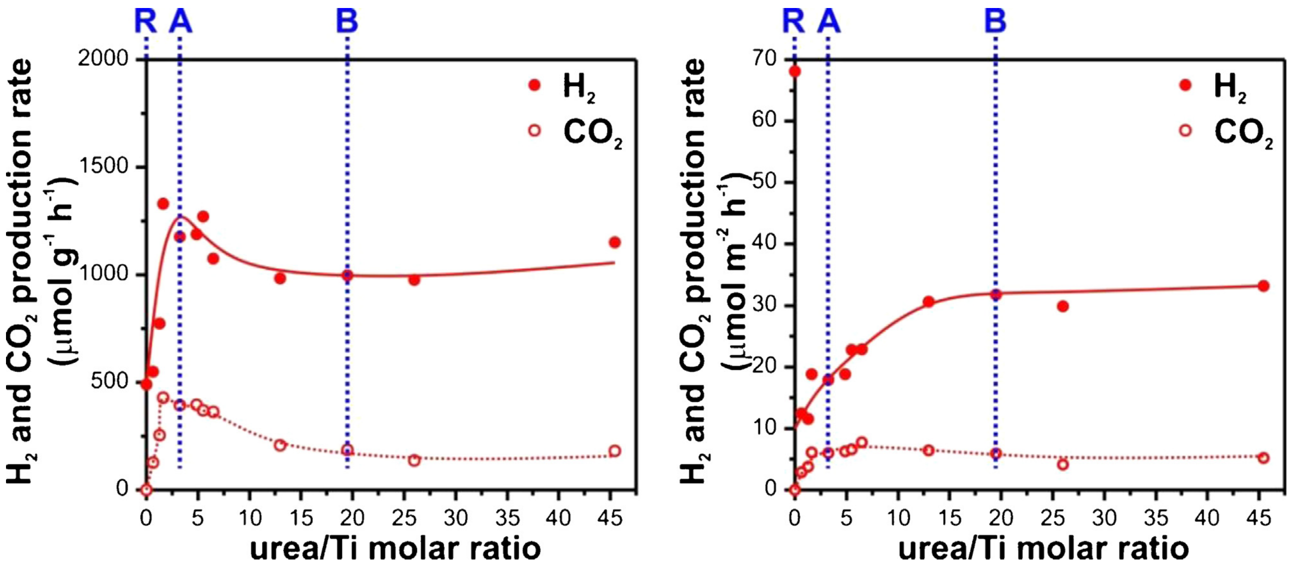

Fig. 5. Stable H_2 and CO_2 production rates by photocatalytic glycerol reforming using Pt(0.2 wt%)/TiO_2 prepared using different urea/Ti molar ratios, normalized with respect to the mass of catalysts (left part) and with respect the surface area (right part). Markers correspond to the urea/Ti molar ratios that allow the preparation of pure phase materials: rutile (R), anatase (A) and brookite (B).

Please cite this article in press as: A. Beltram, et al., Appl. Catal. A: Gen. (2015), http://dx.doi.org/10.1016/j.apcata.2015.09.022

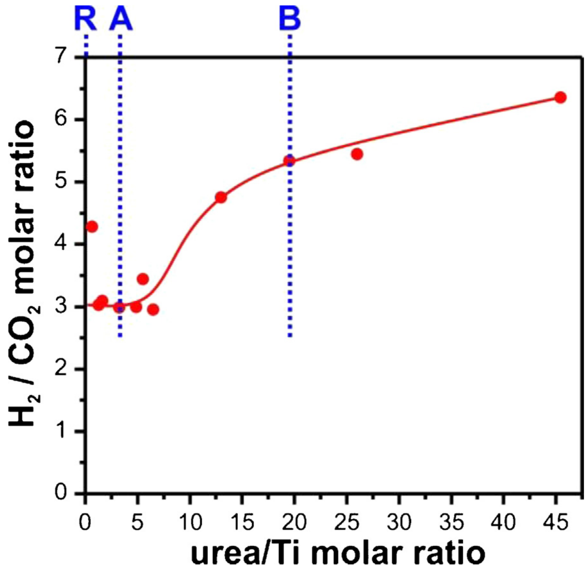

Fig. 6. Stable H_2/CO_2 molar ratio obtained during photocatalytic glycerol reforming using Pt(0.2 wt%)/TiO_2 prepared using different urea/Ti molar ratios. Markers correspond to the urea/Ti molar ratios that allow the preparation of pure phase materials: rutile (R), anatase (A) and brookite (B).

urea/Ti molar ratio employed in the synthesis of the TiO_2 materials. As in the case of ethanol, the maximum production rates normalized with respect to the mass of the photocatalysts (Fig. 5, left part) have been observed for anatase-rich materials (T-1.62–T-5.52) for both H_2 and CO_2. In the case of glycerol, as the urea/Ti molar ratio increases leading to the production of pure brookite, only a moderate decrease in activity is observed for H_2 production while the CO_2 production is deeply affected. Normalizing the H_2 and CO_2 production rates with respect to the surface area of the photocatalysts (Fig. 5, right part), the maximum in H_2 production is observed for brookite-rich materials while the maximum in CO_2 production rate is obtained for anatase-rich samples. Fig. 6 presents the H_2/CO_2 molar ratios obtained after stabilization of the photocatalytic activity, showing a relative minimum for anatase-rich samples. This suggests that anatase phase has best performance in oxidation of by-products and decarboxylation of intermediate carboxylic acids. Notably, the observed H_2/CO_2 molar ratios are always higher than 2.33, the theoretical value corresponding to the complete reforming of glycerol into H_2 and CO_2 following the reaction:

$$C_3H_8O_3 + 3H_2O \rightarrow 7H_2 + 3CO_2$$

The peculiar behavior of T-0 sample (no CO_2 production), in combination with the low surface area of the materials, leads to a very high H_2 production rate when normalized on the surface area. This could result from the combination of various factors, including a different adsorption of glycerol and its by-products on the surface of rutile, a different selectivity in dehydrogenation of the glycerol molecule or the possible availability of a large fraction of active sites for H_2 production (being not involved in organic molecule oxidation).

The results obtained from the gas phase analysis during photocatalytic reforming of glycerol aqueous solutions indicate that significant modifications of the reactivity are induced by the phase conposition of TiO_2 materials, controlled by the urea/Ti molar ratio employed in their synthesis. Anatase-brookite composites are more active that anatase-rutile material in H_2 production thorugh the glycerol photoreforming, as a result of the different conduction band edge potential for the three polymorphs [65,77,78]. At the same time, anatase-rich phases are the most active in oxidation steps of the glycerol photoreforming network, since they demonstrated the higher CO_2 production rates.

The most abundant by-products detected in the liquid phase collected after photocatlaytic experiments are listed in Table S3. The results of the semiquantitative analysis show that CO_2 production takes place essentially through oxidation and decarboxylation of intermediates after dehydrogenation of the primary OH groups of glycerol: 2,3-dihydroxypropanal is observed in very low amounts, indicating that its oxidation and decarboxylation is very fast. 1,3-dihydroxy-2-propanone, 1-hydroxy-2-propanone and a series of dioxanes are produced starting from dehydrogenation of the secondary OH group [53]. Hydroxyacetaldehyde could be produced by C—C bond cleavage and further dehydrogenation following both the reaction pathways. Notably, in the case of the T-0 sample, only by-products deriving through 1,3-dihydroxy-2-propanone formation are observed, suggesting that selective dehydrogenation of glycerol on the secondary OH group is possible on photocatalysts containing rutile.

4. Conclusions

In this study, TiO_2 materials with tunable phase composition have been prepared by thermal hydrolysis of titanium (IV) bis(ammonium lactate) dihydroxyde in the presence of different amounts of urea and used as photocatalysts in the H_2 production from aqueous solution containing ethanol or glycerol under irradiation with simulated sunlight.

Increasing the urea/Ti molar ratio, the phase composition changes from pure rutile to anatase/rutile and finally to pure anatase, leading to a parallel increase of surface area of the materials. Further increase in urea/Ti molar ratio resulted first in the formation of anatase/brookite composite and later to pure brookite above the molar ratio of 19.5, accompanied, however, by a decrease of the surface area of the materials. TEM and XRD analysis revealed that anatase is formed by irregular crystallites with dimensions around 15 nm, while larger particles (60–75 nm) are observed when rutile is present. Moreover, brookite phase is present in the characteristic form of nanorods, 20–40 nm wide and 80–100 nm long. Photodeposition of Pt as co-catalysts resulted in the formation of metal nanoparticles with an average size of 2.0 nm, irrespectively from the phase composition of the support and of sacrificial agent used.

The results from photocatalytic activity evidenced significant differences among the samples. The higher H_2 production on a mass bases was observed for the anatase-rich materials using both ethanol and glycerol as sacrificial agents. Nevertheless, when normalized with respect to the surface area of the photocatalysts, brookite samples showed the higher H_2 productivity, indicating that the facets exposed by brookite, in combination with its favorable electronic properties, are more active for proton reduction. Moreover, a higher H_2/CO_2 ratio was observed during photocatalytic reforming of glycerol using brookite, suggesting that this polymorph is less active in complete mineralization of the organic skeleton and opening interesting opportunities in selective oxidation of the sacrificial agent. Notably, dehydrogenation of glycerol on rutile takes place selectively through the secondary OH group, although with a very low activity.

The results presented in this study confirm that various aspects of the photocatalytic activity of TiO_2 polymorphs have already to be fully clarified with respect to the possible H_2 production through sustainable solar reforming of oxygenated compounds, especially for the less investigated brookite phase. Particular increments on the photocatalytic catalytic activity in H_2 production using brookite is expected after a significant decrease of its crystallite sizes resulting in an increase of its surface area.

Acknowledgements

Dr. E. Aneggi and Prof. A. Trovarelli (University of Udine, Italy) are kindly acknowledged for access to XRD facility. Dr. M. Crosera and Prof. G. Adami (University of Trieste, Italy) are kindly acknowledged for GF-AAS analysis. A.B., I.R.O., T.M. and P.F. acknowledge University of Trieste (Project FRA2013), ICCOM-CNR and INSTM Consortium, MIUR, Italy through the project HI-PHUTURE (protocol 2010N3T9M4) and European Community through the project FP7-NMP-2012-SMALL-6 (project ID 310651) for financial support. J.J. Delgado is grateful to Ramon y Cajal program and the Ce-NanoSurPhases project grant from MINECO ATOMCAT.

Appendix A. Supplementary data

Supplementary data associated with this article can be found, in the online version, at http://dx.doi.org/10.1016/j.apcata.2015.09.022.

References

[1] N. Armaroli, V. Balzani, ChemSusChem 4 (2011) 21.
[2] C.M. Kalamaras, A.M. Efstathiou, Conf. Pap. Energy 2013 (2013) 1.
[3] DOE Hydrogen and Fuel Cells Program: 2014, Annual Progress Report, 2014.
[4] T. Montini, R. Singh, P. Das, B. Lorenzut, N. Bertero, P. Riello, A. Benedetti, G. Giambastiani, C. Bianchini, S. Zinoviev, S. Miertus, P. Fornasiero, ChemSusChem 3 (2010) 619.
[5] T. Montini, L. De Rogatis, V. Gombac, P. Fornasiero, M. Graziani, Appl. Catal. B Environ. 71 (2007) 125.
[6] R.R. Soares, D.A. Simonetti, J.A. Dumesic, Angew. Chem. Int. Ed. 45 (2006) 3982.
[7] R.D. Cortright, R.R. Davda, J.A. Dumesic, Nature 418 (2002) 964.
[8] R.R. Davda, J.W. Shabaker, G.W. Huber, R.D. Cortright, J.A. Dumesic, Appl. Catal. B Environ. 56 (2005) 171.
[9] T. Patterson, S. Esteves, S. Carr, F. Zhang, J. Reed, J. Maddy, A. Guwy, Int. J. Hydrog. Energy 39 (2014) 7190.
[10] A. Kazim, Renew. Energy 35 (2010) 2257.
[11] A. Đukić, Int. J. Hydrog. Energy 40 (2015) 7465.
[12] F.E. Osterloh, Chem. Soc. Rev. 42 (2013) 2294.
[13] S.Y. Reece, J.A. Hamel, K. Sung, T.D. Jarvi, A.J. Esswein, J.J.H. Pijpers, D.G. Nocera, Science 334 (2011) 645.
[14] D.G. Nocera, Acc. Chem. Res. 45 (2012) 767.
[15] S. Bensaid, G. Centi, E. Garrone, S. Perathoner, G. Saracco, ChemSusChem 5 (2012) 500.
[16] S. Abanades, G. Flamant, Sol. Energy 80 (2006) 1611.
[17] A. Steinfeld, Int. J. Hydrog. Energy 27 (2002) 611.
[18] R. Abe, J. Photochem. Photobiol. C Photochem. Rev. 11 (2010) 179.
[19] I. Rossetti, ISRN Chem. Eng. 2012 (2012) 1.
[20] M. Cargnello, A. Gasparotto, V. Gombac, T. Montini, D. Barreca, P. Fornasiero, Eur. J. Inorg. Chem. 2011 (2011) 4309.
[21] J.C. Colmenares, A. Magdziarz, A. Bielejewska, Bioresour. Technol. 102 (2011) 11254.
[22] Y. Ma, X. Wang, Y. Jia, X. Chen, H. Han, C. Li, Chem. Rev. 114 (2014) 9987.
[23] J. Schneider, M. Matsuoka, M. Takeuchi, J. Zhang, Y. Horiuchi, M. Anpo, D.W. Bahnemann, Chem. Rev. 114 (2014) 9919–9986.
[24] K. Wilke, H.D. Breuer, J. Photochem. Photobiol. A Chem. 121 (1999) 49.
[25] H. Yamashita, Y. Ichihashi, M. Takeuchi, S. Kishiguchi, M. Anpo, J. Synchrotron Radiat. 6 (1999) 451.
[26] T. Umebayashi, T. Yamaki, H. Itoh, K. Asai, J. Phys. Chem. Solids 63 (2002) 1909.
[27] D. Dvoranová, V. Brezová, M. Mazúr, M.A. Malati, Appl. Catal. B Environ. 37 (2002) 91.
[28] A. Di Paola, E. Garcıía-López, S. Ikeda, G. Marcı̀, B. Ohtani, L. Palmisano, Catal. Today 75 (2002) 87.
[29] A. Naldoni, M. Allieta, S. Santangelo, M. Marelli, F. Fabbri, S. Cappelli, C.L. Bianchi, R. Psaro, V. Dal Santo, J. Am. Chem. Soc. 134 (2012) 7600.
[30] A. Gallo, T. Montini, M. Marelli, A. Minguzzi, V. Gombac, R. Psaro, P. Fornasiero, V. Dal Santo, ChemSusChem 5 (2012) 1800.
[31] A. Gallo, M. Marelli, R. Psaro, V. Gombac, T. Montini, P. Fornasiero, R. Pievo, V. Dal Santo, Green Chem. 14 (2012) 330.
[32] W.H. Saputera, G. Mul, M.S. Hamdy, Catal. Today 246 (2015) 60.
[33] M.S. Hamdy, R. Amrollahi, G. Mul, ACS Catal. 2 (2012) 2641.
[34] G. Liu, C. Sun, S.C. Smith, L. Wang, G.Q.M. Lu, H.-M. Cheng, J. Colloid Interface Sci. 349 (2010) 477.
[35] G. Liu, H.G. Yang, X. Wang, L. Cheng, J. Pan, G.Q.M. Lu, H.-M. Cheng, J. Am. Chem. Soc. 131 (2009) 12868.
[36] M. Bettinelli, V. Dallacasa, D. Falcomer, P. Fornasiero, V. Gombac, T. Montini, L. Romanò, A. Speghini, J. Hazard. Mater. 146 (2007) 529.
[37] G. Liu, Y. Zhao, C. Sun, F. Li, G.Q. Lu, H.-M. Cheng, Angew. Chem. Int. Ed. Engl. 47 (2008) 4516.
[38] V. Gombac, L. De Rogatis, A. Gasparotto, G. Vicario, T. Montini, D. Barreca, G. Balducci, P. Fornasiero, E. Tondello, M. Graziani, Chem. Phys. 339 (2007) 111.
[39] M. Fittipaldi, V. Gombac, A. Gasparotto, C. Deiana, G. Adami, D. Barreca, T. Montini, G. Martra, D. Gatteschi, P. Fornasiero, ChemPhysChem 12 (2011) 2221.
[40] S.U.M. Khan, M. Al-Shahry, W.B. Ingler, Science 297 (2002) 2243.
[41] L. Lin, W. Lin, Y. Zhu, B. Zhao, Y. Xie, Chem. Lett. 34 (2005) 284.
[42] M.V. Dozzi, E. Selli, J. Photochem. Photobiol. C Photochem. Rev. 14 (2013) 13.
[43] M. Guo, L. Li, H. Lin, Y. Zuo, X. Huang, G. Li, Chem. Commun. (Camb.) 49 (2013) 11752.
[44] Y. Ma, R. Chong, F. Zhang, Q. Xu, S. Shen, H. Han, C. Li, Phys. Chem. Chem. Phys. 16 (2014) 17734.
[45] C. Wang, R.L. Thompson, J. Baltrus, C. Matranga, J. Phys. Chem. Lett. 1 (2010) 48.
[46] I. Robel, M. Kuno, P.V. Kamat, J. Am. Chem. Soc. 129 (2007) 4136.
[47] Y. Zhu, Z. Chen, T. Gao, Q. Huang, F. Niu, L. Qin, P. Tang, Y. Huang, Z. Sha, Y. Wang, Appl. Catal. B Environ. 163 (2015) 16.
[48] R. Baba, S. Nakabayashi, A. Fujishima, K. Honda, J. Phys. Chem. 89 (1985) 1902.
[49] V. Subramanian, E. Wolf, P.V. Kamat, J. Phys. Chem. B 105 (2001) 11439.
[50] V. Subramanian, E.E. Wolf, P.V. Kamat, J. Am. Chem. Soc. 126 (2004) 4943.
[51] A.W. Maijenburg, J. Veerbeek, R. de Putter, S.A. Veldhuis, M.G.C. Zoontjes, G. Mul, J.M. Montero-Moreno, K. Nielsch, H. Schäfer, M. Steinhart, J.E. ten Elshof, J. Mater. Chem. A 2 (2014) 2648.
[52] C. Ampelli, R. Passalacqua, C. Genovese, S. Perathoner, G. Centi, T. Montini, V. Gombac, J.J. Delgado Jaen, P. Fornasiero, RSC Adv. 3 (2013) 21776.
[53] T. Montini, V. Gombac, L. Sordelli, J.J. Delgado, X. Chen, G. Adami, P. Fornasiero, ChemCatChem 3 (2011) 574.
[54] W. Chen, Y. Lu, W. Dong, Z. Chen, M. Shen, Mater. Res. Bull. 50 (2014) 31.
[55] J. Li, H. Zhou, S. Qian, Z. Liu, J. Feng, P. Jin, X. Liu, Appl. Phys. Lett. 104 (2014) 261110.
[56] J.S. DuChene, B.C. Sweeny, A.C. Johnston-Peck, D. Su, E.A. Stach, W.D. Wei, Angew. Chem. Int. Ed. Engl. 53 (2014) 7887.
[57] J. Chen, D. Yang, D. Song, J. Jiang, A. Ma, M.Z. Hu, C. Ni, J. Power Sources 280 (2015) 649.
[58] J. Sá, G. Tagliabue, P. Friedli, J. Szlachetko, M.H. Rittmann-Frank, F.G. Santomauro, C.J. Milne, H. Sigg, Energy Environ. Sci. 6 (2013) 3584.
[59] L. Amidani, A. Naldoni, M. Malvestuto, M. Marelli, P. Glatzel, V. Dal Santo, F. Boscherini, Angew. Chem. Int. Ed. 54 (2015) 5413.
[60] A. Naldoni, F. Fabbri, M. Altomare, M. Marelli, R. Psaro, E. Selli, G. Salviati, V. Dal Santo, Phys. Chem. Chem. Phys. 17 (2015) 4864.
[61] J. Zhang, X. Chen, Y. Shen, Y. Li, Z. Hu, J. Chu, Phys. Chem. Chem. Phys. 13 (2011) 13096.
[62] A. Di Paola, M. Bellardita, R. Ceccato, L. Palmisano, F. Parrino, J. Phys. Chem. C 113 (2009) 15166.
[63] J. Cihlar, V. Kasparek, M. Kralova, K. Castkova, Int. J. Hydrog. Energy 40 (2015) 2950.
[64] T.A. Kandiel, A. Feldhoff, L. Robben, R. Dillert, D.W. Bahnemann, Chem. Mater. 22 (2010) 2050.
[65] Q. Tay, X. Liu, Y. Tang, Z. Jiang, T.C. Sum, Z. Chen, J. Phys. Chem. C 117 (2013) 14973.
[66] I. Romero Ocaña, A. Beltram, J.J. Delgado Jaén, G. Adami, T. Montini, P. Fornasiero, Inorg. Chim. Acta 431 (2015) 197.
[67] H. Zhao, L. Liu, J.M. Andino, Y. Li, J. Mater. Chem. A 1 (2013) 8209.
[68] G. Carraro, C. Maccato, A. Gasparotto, T. Montini, S. Turner, O.I. Lebedev, V. Gombac, G. Adami, G. Van Tendeloo, D. Barreca, P. Fornasiero, Adv. Funct. Mater. 24 (2014) 372.
[69] H. Kisch, D. Bahnemann, J. Phys. Chem. Lett. 6 (2015) 1907.
[70] S.G. Kumar, K.S.R.K. Rao, Nanoscale 6 (2014) 11574.
[71] B. Zhao, L. Lin, D. He, J. Mater. Chem. A 1 (2013) 1659.
[72] T. Ohno, T. Higo, N. Murakami, H. Saito, Q. Zhang, Y. Yang, T. Tsubota, Appl. Catal. B Environ. 152–153 (2014) 309.
[73] K.S.W. Sing, D.H. Everett, R.A.W. Haul, L. Moscou, R.A. Pierotti, J. Rouquerol, T. Siemieniewska, Pure Appl. Chem. 57 (1985) 603.
[74] A. Sivasamy, K.Y. Cheah, P. Fornasiero, F. Kemausuor, S. Zinoviev, S. Miertus, ChemSusChem 2 (2009) 278.
[75] A. Patsoura, D.I. Kondarides, X.E. Verykios, Catal. Today 124 (2007) 94.
[76] Y. Liu, Z. Wang, W. Wang, W. Huang, J. Catal. 310 (2014) 16.
[77] G. Chiarello, E. Selli, L. Forni, Appl. Catal. B Environ. 84 (2008) 332.
[78] M. Kapilashrami, Y. Zhang, Y.-S. Liu, A. Hagfeldt, J. Guo, Chem. Rev. 114 (2014) 9662.
[79] D.C. Hurum, A.G. Agrios, K.A. Gray, T. Rajh, M.C. Thurnauer, J. Phys. Chem. B 107 (2003) 4545.
[80] M. Murdoch, G.I.N. Waterhouse, M.A. Nadeem, J.B. Metson, M.A. Keane, R.F. Howe, J. Llorca, H. Idriss, Nat. Chem. 3 (2011) 489.
[81] H. Zhang, J.F. Banfield, J. Phys. Chem. B 104 (2000) 3481.
[82] M.A. Nadeem, M. Murdoch, G.I.N. Waterhouse, J.B. Metson, M.A. Keane, J. Llorca, H. Idriss, J. Photochem. Photobiol. A Chem. 216 (2010) 250.
[83] L. Zhang, V.M. Menendez-Flores, N. Murakami, T. Ohno, Appl. Surf. Sci. 258 (2012) 5803.
[84] T. Ohno, K. Sarukawa, M. Matsumura, New J. Chem. 26 (2002) 1167.
[85] Y. Yang, C. Chang, H. Idriss, Appl. Catal. B Environ. 67 (2006) 217.
[86] A.V. Puga, A. Forneli, H. García, A. Corma, Adv. Funct. Mater. 24 (2014) 241.